The Planetary Science Journal, 4:236 (14pp), 2023 December https://doi.org/10.3847/PSJ/ad0a64

Optical Monitoring of the Didymos–Dimorphos Asteroid System with the Danish Telescope around the DART Mission Impact

Agata Rożek[1], Colin Snodgrass[1], Uffe G. Jørgensen[2], Petr Pravec[3], Mariangela Bonavita[1], Markus Rabus[4], Elahe Khalouei[5], Penélope Longa-Peña[6], Martin J. Burgdorf[7], Abbie Donaldson[1], Daniel Gardener[1], Dennis Crake[1], Sedighe Sajadian[8], Valerio Bozza[9,10], Jesper Skottfelt[11], Martin Dominik[12], J. Fynbo[13], Tobias C. Hinse[14], Markus Hundertmark[15], Sohrab Rahvar[16], John Southworth[17], Jeremy Tregloan-Reed[18], Mike Kretlow[19], Paolo Rota[9,10], Nuno Peixinho[20], Michael Andersen[13], Flavia Amadio[2], Daniela Barrios-López[6], and Nora Soledad Castillo Baeza[6]

[1] Institute for Astronomy, University of Edinburgh, Royal Observatory, Edinburgh EH9 3HJ, UK; a.rozek@ed.ac.uk
[2] Centre for ExoLife Sciences, Niels Bohr Institute, University of Copenhagen, Øster Voldgade 5, DK-1350 Copenhagen, Denmark
[3] Astronomical Institute of the Academy of Sciences of the Czech Republic, Fričova 298, Ondřejov CZ-25165, Czech Republic
[4] Departamento de Matemática y Física Aplicadas, Facultad de Ingeniería, Universidad Católica de la Santísima Concepción, Alonso de Rivera 2850, Concepción, Chile
[5] Astronomy Research Center, Research Institute of Basic Sciences, Seoul National University, 1 Gwanak-ro, Gwanak-gu, Seoul 08826, Republic of Korea
[6] Centro de Astronomía, Universidad de Antofagasta, Av. Angamos 601, Antofagasta, Chile
[7] Universität Hamburg, Faculty of Mathematics, Informatics and Natural Sciences, Department of Earth Sciences, Meteorological Institute, Bundesstraße 55, D-20146 Hamburg, Germany
[8] Department of Physics, Isfahan University of Technology, Isfahan 84156-83111, Iran
[9] Dipartimento di Fisica "E.R. Caianiello,"Università di Salerno, Via Giovanni Paolo II 132, I-84084 Fisciano, Italy
[10] Istituto Nazionale di Fisica Nucleare, Sezione di Napoli, Strada Comunale Cinthia, I-80126 Napoli, Italy
[11] Centre for Electronic Imaging, School of Physical Sciences, The Open University, Milton Keynes MK7 6AA, UK
[12] University of St Andrews, Centre for Exoplanet Science, SUPA School of Physics & Astronomy, North Haugh, St Andrews KY16 9SS, UK
[13] Niels Bohr Institute, University of Copenhagen, Blegdamsvej 17, DK-2100 Copenhagen, Denmark
[14] University of Southern Denmark, Department of Physics, Chemistry and Pharmacy, Campusvej 55, DK-5230 Odense M, Denmark
[15] Astronomisches Rechen-Institut, Zentrum für Astronomie der Universität Heidelberg (ZAH), D-69120 Heidelberg, Germany
[16] Department of Physics, Sharif University of Technology, P.O. Box 11155-9161, Tehran, Iran
[17] Astrophysics Group, Keele University, Staffordshire ST5 5BG, UK
[18] Instituto de Astronomia y Ciencias Planetarias de Atacama, Universidad de Atacama, Copayapu 485, Copiapo, Chile
[19] Instituto de Astrofísica de Andalucía, Granada, Spain
[20] Instituto de Astrofísica e Cêcias do Espaço, Departamento de Física, Universidade de Coimbra, PT3040-004 Coimbra, Portugal
Received 2023 August 17; revised 2023 October 13; accepted 2023 November 3; published 2023 December 12

Abstract

The NASA's Double-Asteroid Redirection Test (DART) was a unique planetary defence and technology test mission, the first of its kind. The main spacecraft of the DART mission impacted the target asteroid Dimorphos, a small moon orbiting the asteroid Didymos (65803), on 2022 September 26. The impact brought up a mass of ejecta which, together with the direct momentum transfer from the collision, caused an orbital period change of 33 ± 1 minutes, as measured by ground-based observations. We report here the outcome of the optical monitoring campaign of the Didymos system from the Danish 1.54 m telescope at La Silla around the time of impact. The observations contributed to the determination of the changes in the orbital parameters of the Didymos–Dimorphos system, as reported by Thomas et al., but in this paper we focus on the ejecta produced by the DART impact. We present photometric measurements from which we remove the contribution from the Didymos–Dimorphos system using an *H–G* photometric model. Using two photometric apertures we determine the fading rate of the ejecta to be 0.115 ± 0.003 mag day^{-1} (in a 2″ aperture) and 0.086 ± 0.003 mag day^{-1} (5″) over the first week postimpact. After about 8 days postimpact we note the fading slows down to 0.057 ± 0.003 mag day^{-1} (2″ aperture) and 0.068 ± 0.002 mag day^{-1} (5″). We include deep-stacked images of the system to illustrate the ejecta evolution during the first 18 days, noting the emergence of dust tails formed from ejecta pushed in the antisolar direction, and measuring the extent of the particles ejected Sunward to be at least 4000 km.

Unified Astronomy Thesaurus concepts: Light curves (918); Asteroid satellites (2207); Apollo group (58); Planetary probes (1252)

Supporting material: machine-readable table

1. Introduction

The Double-Asteroid Redirection Test (DART) mission was a world-first practical planetary defense test (Rivkin et al. 2021). The DART spacecraft was a 580 kg probe that crashed into the asteroid Dimorphos, a small moon of the asteroid Didymos, on 2022 September 26 at 23:14:24.183 UTC (Daly et al. 2023). One of the principal aims of the DART mission was to change the orbital period of Dimorphos around Didymos in a measurable way, in order to understand and quantify the effect of collisions on near-Earth objects, with the long-term aim of getting a deeper understanding about humanity's possibility to protect Earth against a potential future asteroid impact. This goal was successfully achieved

Table 1
List of the Light Curves of Asteroid (65803) Didymos Presented in This Study

UT Date (yyyy-mm-dd) (hh:mm:ss.s)	JD	Len. (hr)	Exp. (s)	Seeing (″)	$R_\odot$ (au)	Δ (au)	α (°)	$V_{\rm mag}$ (mag)	λ_o (°)	β_o (°)
2022-Sep-16 09:08:28.8	2459838.881	1.5	10	1.9	1.078	0.096	38.9	14.696	5.2	−41
2022-Sep-20 06:10:37.5	2459842.757	7.1	20	3	1.065	0.087	43.7	14.585	13.8	−44.8
2022-Sep-25 06:34:11.2	2459847.774	6.2	7	2.6	1.051	0.078	50.7	14.508	29.3	−48.9
2022-Sep-26 04:22:05.4	2459848.682	1	7	2	1.048	0.077	52.1	14.511	32.7	−49.4
2022-Sep-27 06:26:22.5	2459849.768	6.7	7	1.6	1.045	0.075	53.7	14.492	36.9	−49.8
2022-Sep-28 04:56:46.6	2459850.706	4.7	7	1.9	1.043	0.074	55.1	14.498	40.7	−50.1
2022-Sep-29 06:14:03.9	2459851.76	6.8	7	1.6	1.04	0.073	56.7	14.507	45.1	−50.2
2022-Sep-30 06:09:33.7	2459852.757	7.2	7	1.8	1.038	0.073	58.2	14.545	49.3	−50.2
2022-Oct-01 07:46:07.1	2459853.824	3.8	6	1.5	1.036	0.072	59.7	14.556	53.9	−49.9
2022-Oct-02 06:05:12.0	2459854.754	4.9	6	1.3	1.034	0.072	61.1	14.592	57.8	−49.6
2022-Oct-03 04:57:55.7	2459855.707	1	6	1.5	1.032	0.071	62.5	14.598	61.8	−49
2022-Oct-04 04:09:00.9	2459856.673	1.2	6	2.1	1.03	0.071	63.8	14.634	65.8	−48.3
2022-Oct-05 04:46:03.0	2459857.699	2.2	12	2.8	1.028	0.071	65.2	14.671	69.8	−47.4
2022-Oct-06 07:13:05.3	2459858.801	4.5	10	2.8	1.026	0.071	66.6	14.710	73.9	−46.3
2022-Oct-07 06:19:18.5	2459859.763	4.3	8	1.6	1.024	0.072	67.8	14.773	77.4	−45.2
2022-Oct-08 06:45:27.6	2459860.782	5.5	7	2.5	1.023	0.072	69	14.807	80.8	−44
2022-Oct-09 08:00:16.0	2459861.834	2.6	9	1.9	1.021	0.073	70.1	14.868	84.1	−42.6
2022-Oct-10 06:55:51.5	2459862.789	4.8	8	2.4	1.02	0.074	71.1	14.926	86.9	−41.3
2022-Oct-11 04:56:57.4	2459863.706	1.1	7	2.4	1.019	0.075	71.9	14.981	89.4	−40.1
2022-Oct-12 08:26:12.7	2459864.852	1.2	10	1.7	1.018	0.076	72.8	15.037	92.3	−38.4
2022-Oct-13 08:25:17.0	2459865.851	1.1	8	1.8	1.017	0.077	73.6	15.088	94.7	−37
2022-Oct-14 07:44:41.3	2459866.823	0.8	8	1.7	1.016	0.078	74.2	15.134	96.8	−35.6

Notes. The table includes details of each light curve collected in our Didymos observing campaign. All light curves were collected in the Bessel *R* filter. The columns list the observing circumstances for each night: universal Time (UT), "Date," and Julian Date ("JD") at the middle of the exposure series taken on a given night, the total length ("Len." in hours) of the observing sequence, the exposure time ("Exp." in seconds) of the individual images in the sequence, the approximate "Seeing" (in arcseconds), estimated based on the FWHM of selected background stars, the heliocentric ("$r_\odot$") and geocentric ("Δ") distances measured in astronomical units, the solar phase angle ("α"), the apparent "$V_{\rm mag}$" brightness as predicted with the $H = 18.16$, $G = 0.2$ model, (Pravec et al. 2012), and the observer-centered ecliptic longitude ("λ_o") and latitude ("β_o"). Each row represents a single-night light curve which is divided into multiple segments if it spans more than about an hour. The horizontal line splits the preimpact and postimpact data sets.

(Cheng et al. 2023; Thomas et al. 2023). On top of the primary goals, the mission also provided a number of unique opportunities to study other science questions related to asteroids. For example, it provided a rare insight into the mechanics of asteroid collisions that happen naturally in the solar system, but for which we have mostly indirect evidence in the dynamical structure of the main asteroid belt (more specifically the asteroid families; see, e.g., the reviews by Michel et al. 2015; Nesvorný et al. 2015) and the rubble-pile appearance of asteroids (discussed extensively, for example by Walsh 2018; Michel et al. 2020). Direct observations of the dust ejected by the impact, which we will refer to as an ejecta cloud, postimpact can also be used to investigate active asteroids, objects on typically asteroidal orbits displaying activity. The possible activity scenarios for this type of object include outgassing, mass shedding, and recent impacts (e.g., Jewitt et al. 2015, and references therein). While the features of sublimation-driven activity are well studied in the context of comets, asteroid impacts present transient events that are impossible to predict and thus monitor early on. The DART impact was therefore a rare opportunity to collect observations of the formation of an ejecta cloud and tail virtually from the moment of collision. The immediate impact aftermath was observed by the Light Italian Cubesat for Imaging of Asteroids (LICIACube) that accompanied the DART spacecraft (Dotto & Zinzi 2023; Dotto et al. 2023) and further measurements were made with various telescopes, for example by the Hubble Space Telescope (HST; Jewitt et al. 2023; Li et al. 2023), the 8 m Very Large Telescope in Chile (Murphy et al. 2023; Opitom et al. 2023), an array of smaller facilities (Kareta et al. 2023; Lin et al. 2023; Lister et al. 2023; Moskovitz et al. 2023; Polishook et al. 2023), and by amateur astronomers (Graykowski et al. 2023). We report on our observations obtained as a part of this global campaign. In Section 2 we summarize the data collected in our photometric monitoring campaign with the Danish (DK) 1.54 m telescope, as part of the MiNDSTEp consortium that operates the telescope for 6 months each year. In Section 3 we present results of our light-curve analysis, reporting the dimming rate of the ejecta. Finally, in Section 4 we discuss the morphology of the ejecta cloud and tail that formed after the impact, as imaged through the first 18 days after the impact.

2. Observations

We observed the Didymos–Dimorphos system with the DK 1.54 m telescope, located at La Silla observatory in Chile (MPC code W74). The Danish Faint Object Spectrograph and Camera (DFOSC) instrument, with field of view $13\farcm5 \times 13\farcm5$, was used in imaging mode. A series of images in the Bessel *R* filter were taken on each observing night, as listed in Table 1. The object was moving rapidly across the field, but we decided to use sidereal tracking and short exposures to keep both the asteroid and the background stars from trailing. In order to maintain consistency of the relative photometry and monitor the ejecta features, the field was regularly adjusted to keep the asteroid within the central area of the detector while maximizing the overlap between background stars in any

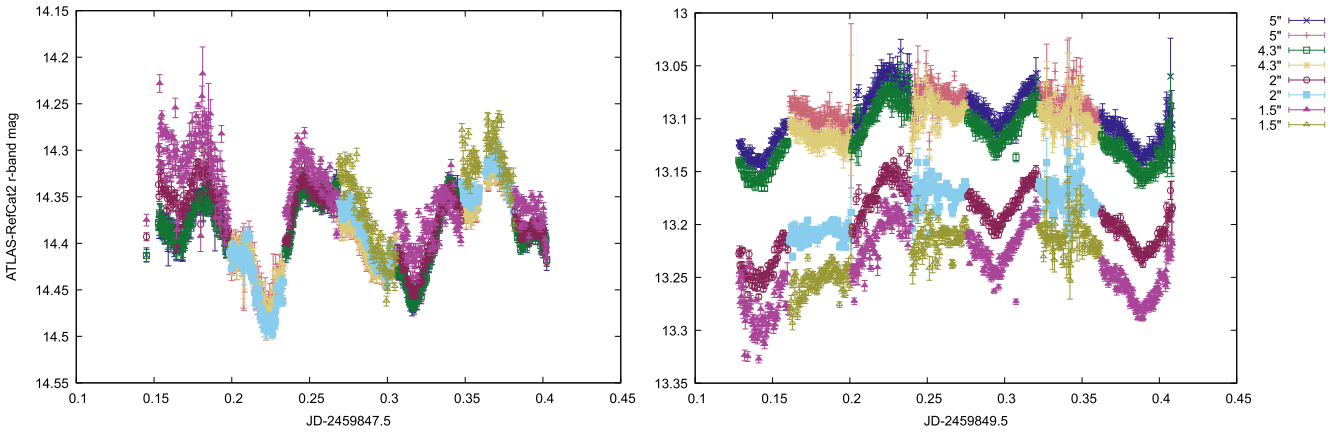

(a) 25 September 2022 (b) 27 September 2022

Figure 1. A sample of multiaperture light curves collected with the DK telescope, calibrated to ATLAS-RefCat2 *r* band. Panel (a) shows an example preimpact light curve (taken with the four fixed-angular-size apertures discussed in the main text), and panel (b) shows an example multiaperture postimpact light curve. The horizontal axis scale is in days since 00:00 UT of a given observing night. Each night is divided into "segments" corresponding to different background fields used for relative light-curve extraction. Each segment and aperture size is marked with a different set of colors and symbols. The full light-curve data set is presented in Figures A1 and A2.

sequence of observations. For the purpose of performing relative photometry the light curves were divided into individual "segments." The main practical difference between the segments is the selection of background stars available. The light-curve segments were usually around 1 hr long, but the exact time they covered depended on how often the observers changed the field.

2.1. Light-curve Extraction

The data reduction and photometry were performed using custom Python procedures utilizing *astropy* (Astropy Collaboration et al. 2013, 2018, 2022). Imaging frames were reduced using standard methods in CCD imaging: bias subtraction and flat-field correction using twilight flats. The asteroid brightness was measured relative to the background stars in each image. Between five and 10 stars were selected fulfilling two criteria: they were not as bright as to be overexposed and had a catalog color $(g-r)<1.5$ (or <1.2 whenever a sufficient number of stars fulfilling this criterion were available). The stellar and asteroid brightnesses were measured using aperture photometry. Due to large amount of ejecta observed in the weeks after the impact, and to ensure consistency with other data sets used for photometric study of the system (Thomas et al. 2023), we decided to use a few fixed-on-sky-size apertures, namely $1\farcs5$, $2''$, $4\farcs3$, and $5''$. We note that due to the seeing conditions throughout our campaign (Table 1) there is little difference between the measurements made in the $1\farcs5$ and $2''$ apertures. Similarly, the photometry in $4\farcs3$ and $5''$ gives comparable results, as both include considerable contribution from the sunlight reflected by the dispersing ejecta cloud. However there is a noticeable difference in the photometric behavior of the system between the small apertures, at the order of seeing, and photometry in larger apertures; so in the further discussion below we will focus on the $2''$ and $5''$ radius apertures. In Table A1 (available online) we present the individual light-curve segments calibrated to the ATLAS-RefCat2 *r*-band magnitudes with the calviacat Python package (Tonry et al. 2018; Kelley & Lister 2022) using the methods outlined by Donaldson et al. (2023). For the purpose of extracting a relative light curve we used the same set of comparison stars as for the calibration. While computing the calibrated magnitude for the asteroid system the color $(g-r)=0.52$ was adopted (Pravec et al. 2022).

2.2. Morphology Extraction

To illustrate the changing dust environment of the Didymos–Dimorphos system we have used the *Gnuastro* software suite (Akhlaghi & Ichikawa 2015; Akhlaghi 2019) to create deep-stacked images for each hour on the first night postimpact and for each night in the rest of the sequence. We used the *NoiseChisel* routine to remove the background sky from images before stacking and then cropped to create 501×501 pixel images on the first night and 701×1501 images for the entire sequence, keeping Didymos always in the same place in the new frames. The images were then combined by taking the sigma-clipped mean value for each pixel. This helped remove the contribution from background stars trailing across the faint ejecta features. The images were then processed with *NoiseChisel*. This subroutine was designed for detection of low-surface-brightness features in the analysis of extragalactic observations. We tested it here to be used as a method of "activity" assessment for the Didymos–Dimorphos system. The subroutine carves out the signal close to the background level by comparing the statistical properties of pixel values in pixels adjacent to an initial high signal-to-noise-ratio detection with statistical properties of the detection-free background. We use this method to investigate the shape of the dust cloud surrounding the asteroid system postimpact.

3. Light-curve Analysis

The contribution of ejecta to the postimpact light curve is immediately apparent. Before the impact, the asteroid brightness measurements were independent of the aperture size within the photometric error bars. From the night of impact there is a clear offset between the brightness measured in different apertures (Figure 1; Appendix Figures A1 and A2). The extent of the ejecta cloud and the eventual emergence of the ejecta tail made it impractical to attempt setting up an aperture that would encompass all of the ejecta. The light curve

Table 2
Outputs of the Photometric Monitoring of the Asteroid (65803) Didymos with the DK 1.54 m Telescope

UT Date (yyyy-mm-dd)	Midseq. Time (day) Since Impact	$H(1, 1, \alpha)_{2''}$ (mag)	$\mathrm{rms}_{2''}$ (mag)	$H(1, 1, \alpha)_{5''}$ (mag)	$\mathrm{rms}_{5''}$ (mag)	$\Delta H_{2''}$ (mag)	$\Delta H_{5''}$ (mag)	$l_{\odot}$ (km)	$l_{-\odot}$ (km)
2022-Sep-16	−10.58717	19.703	0.051	⋯	⋯	0.081	⋯		
2022-Sep-20	−6.71068	19.919	0.050	19.849	0.044	0.168	0.098		
2022-Sep-25	−1.69432	20.064	0.044	20.073	0.039	0.124	0.133		
2022-Sep-26	−0.78605	20.127	0.043	20.118	0.048	0.150	0.141		
2022-Sep-27	0.30026	18.961	0.027	18.865	0.023	−1.060	−1.157	3200	3500
2022-Sep-28	1.23803	19.021	0.013	18.949	0.014	−1.039	−1.111	2500	6900
2022-Sep-29	2.29171	19.193	0.021	19.100	0.018	−0.912	−1.006	4200	
2022-Sep-30	3.28858	19.365	0.029	19.236	0.022	−0.782	−0.912	3800	14,900
2022-Oct-01	4.35563	19.530	0.021	19.374	0.019	−0.663	−0.819	3300	13,500
2022-Oct-02	5.28555	19.659	0.025	19.469	0.023	−0.573	−0.764	3800	15,400
2022-Oct-03	6.23883	19.794	0.031	19.582	0.025	−0.479	−0.692	2100	6500
2022-Oct-04	7.20487	19.893	0.033	19.664	0.024	−0.420	−0.649	2100	5700
2022-Oct-05	8.23059	19.906	0.051	19.662	0.037	−0.449	−0.693	1900	7800
2022-Oct-06	9.33270	20.086	0.043	19.817	0.031	−0.312	−0.581	2200	14,500
2022-Oct-07	10.29535	20.228	0.053	19.940	0.034	−0.206	−0.494	2500	10,900
2022-Oct-08	11.31351	20.321	0.037	20.050	0.029	−0.150	−0.421	1900	11,700
2022-Oct-09	12.36546	20.394	0.028	20.134	0.023	−0.112	−0.372	2200	9400
2022-Oct-10	13.32073	20.515	0.055	20.256	0.040	−0.022	−0.281	1500	11,200
2022-Oct-11	14.23816	20.586	0.038	20.350	0.033	0.021	−0.214	⋯	7400
2022-Oct-12	15.38348	20.679	0.049	20.454	0.056	0.085	−0.141	⋯	⋯
2022-Oct-13	16.38283	20.734	0.040	20.523	0.032	0.115	−0.096	1300	⋯
2022-Oct-14	17.35464	20.798	0.037	20.607	0.031	0.158	−0.033	⋯	⋯

Notes. The first column is the UT date at which the observations were taken, for easy linking with Table 1. Second column, labeled "Midseq. time," shows the time (in days) since the DART mission impact (which happened at JD = 2459849.46806) at the middle of the observing sequence. The columns labeled $H(1, 1, \alpha)$ include the Johnson V mean magnitude for an observing sequence reduced to 1 au heliocentric and geocentric distance, measured in 2″ and 5″ radius apertures. The rms column illustrates the scatter of the measurements going into the mean brightness, which comes from both measurement uncertainties and shape effects. The ΔH columns include the excess brightness (as compared with the $H = 18.16$, $G = 0.2$ model; Pravec et al. 2012). The final two columns illustrate the estimated lower limit on the extent of the postimpact dust cloud in the Sunward ($l_{\odot}$) and antisolar ($l_{-\odot}$) directions. The dust cloud extents were measured using the *NoiseChisel* low-surface-brightness feature extraction tool. Note that the listed dust cloud extents are generally underestimated in the antisolar direction, as explained in detail in the main text.

thus includes the effects due to the shape and rotation of Didymos, mutual eclipses between Didymos and Dimorphos, and the ejecta. Short-term variations (i.e., over the course of a few hours in a single night) are dominated by the first two elements, and the ejecta contribution can be approximated as a constant to allow light-curve decomposition methods to be applied (e.g., Pravec et al. 2006). The results of this analysis were used to measure the change in Dimorphos' orbital period and are described elsewhere (Scheirich et al. 2023; Thomas et al. 2023).

In order to investigate the long-term photometric behavior of the ejecta we have taken the average brightness from each night, translated it to the Johnson V-band system by approximating the ATLAS-RefCat2 r band with PanSTARRS r band and using the correction $(V - r) = 0.248$, where $(V - r)$ is the difference between the Johnson V magnitude and our calibrated r magnitude. The correction is estimated using $(g - r) = 0.52$ for Didymos (Pravec et al. 2022), and a relevant formula from Tonry et al. (2012). The conversion to Johnson V magnitude was needed to facilitate comparison with photometric models that are usually expressed in this system (e.g., Pravec et al. 2012). We then reduce the V magnitude to 1 au distance from the Sun and Earth, i.e., the $H(1, 1, \alpha)$ magnitude. The $H(1, 1, \alpha)$ magnitude measurements made in the 2″ radius aperture as well as in the 5″ radius aperture are summarized in Table 2. Between the preimpact observations and the night of impact the brightness increased by about 1.3 mag in the 5″ aperture, and by 1.2 mag in the 2″ aperture relative to what was expected from preimpact photometric models and measured shortly before the impact (Figure 2). The brightness then faded at 0.105 ± 0.002 mag day^{-1} in the 5″ aperture, and at a slightly quicker rate of 0.133 ± 0.001 mag day^{-1} in the 2″ aperture, until about 8 days postimpact. At that time the system brightness jumped by about 0.2 mag above the expected trend in all apertures, but continued fading after the event. Interestingly, the fading rate measured between day nine and 18 is quicker in the 5″ aperture (0.120 ± 0.002 mag day^{-1}) than in the 2″ aperture (0.109 ± 0.002 mag day^{-1}).

The fading brightness is a combination of several factors: the solar phase angle at which the system is observed is increasing, with the asteroid moving away from Earth the size (measured in kilometers) of the aperture is getting smaller; and the amount of detectable ejecta in each aperture is varying due to movement of the ejecta. The variation of the ejecta flow and brightness is of the highest interest in the context of the DART impact event. However, in order to make this kind of measurement, it is necessary to first subtract the non–ejecta-related brightness variations from the observed values. To this purpose we include the two (preimpact) photometric models, described with the absolute magnitude at zero phase angle (H) and slope parameter (G), as the two curves in the lower part of Figure 2 (a). The upper of these two lines represents the $H = 18.12$, $G = 0.15$ model that is used to provide brightness estimates in the Horizons ephemerides system,[21] while the lower of the two lines is the $H = 18.16$, $G = 0.2$ model from Pravec et al. (2012). We note that both the literature model and

[21] https://ssd.jpl.nasa.gov/horizons/

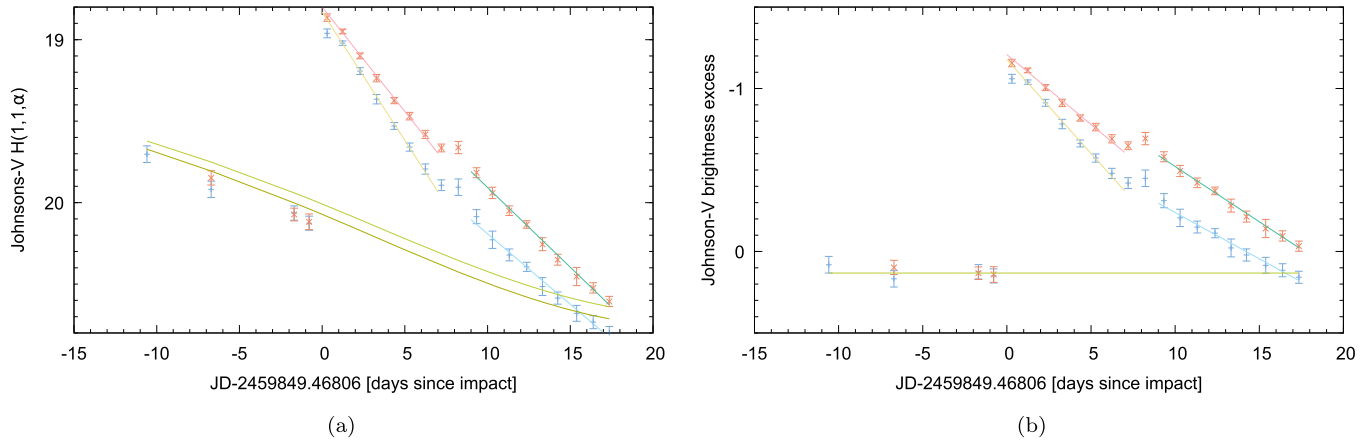

(a) (b)

Figure 2. The figure shows the apparent fading of the Didymos–Dimorphos system in the Johnson *V* band. The blue crosses represent the averaged brightness in the 2″ aperture for each night and red "*x*" symbols correspond to the brightness in the 5″ aperture. Panel (a) shows the heliocentric- and geocentric-distance-corrected brightness of the asteroids and ejecta cloud. The straight colored lines represent linear trend fits to subsets of data and the curved lines show the asteroid brightness as predicted by the photometric models. In panel (b) we remove the contribution from the Didymos–Dimorphos system by using the photometric model from Pravec et al. (2012) and remeasure the brightness fading rates—illustrated again with colored straight lines; the horizontal line illustrates the straight-line fit to the preimpact photometry.

the solution adapted in the Horizons ephemerides system overestimate the brightness of the Didymos–Dimorphos system before impact; the measured system brightness is below both lines. This is likely due to the unusually large phase angles at which the observations were collected. The data that were used for the determination of the $H = 18.16$, $G = 0.2$ model covered phase angles of 2–40° (Kitazato et al. 2004; Pravec et al. 2006) while in the time span of our observations the solar-phase-angle changes from about 50° around the time of impact to 75° at the end of the sequence. The magnitudes from the model by Pravec et al. (2012) are in better agreement with our observed preimpact magnitudes of the system than the alternative Horizons-model (while both models agree with our determined slope in the preimpact magnitudes). We therefore adopt the Pravec et al. (2012) model to deduce the brightness excess due to ejecta alone (Figure 2(b)). Measurement of the preimpact light curves shows that the asteroid's brightness was overestimated by the model by about 0.132 ± 0.018 mag. The fading trends are shallower when measured on just the brightness excess alone, and also change around the 8 day mark. The fading slows down, from initially being 0.115 ± 0.003 mag day^{-1} (in the 2″ aperture) and 0.086 ± 0.003 mag day^{-1} (in the 5″ aperture) over the first week to 0.057 ± 0.003 mag day^{-1} (2″) and 0.068 ± 0.002 mag day^{-1} (5″). This fading rate convolves the rate of ejecta escaping the system with solar-phase-angle effects that are different for different ejecta size regimes (Lolachi et al. 2023). In the phase-angle regime covered by our observations the brightness of very fine submillimeter material should appear to increase slightly, while for larger (millimeter to centimeter) material it should drop, and drop even faster for larger boulders (meter sized) and for the asteroids themselves. For a typical cometary coma phase function (Schleicher & Bair 2011), which is dominated by micron-scale grains, the same reflecting area of dust would appear ∼17% brighter due to the changing phase angle observed between the impact and mid-October. Over the same phase-angle range, the brightness of the larger material (according to the *H–G* photometric model) reduces by ∼43%.

HST and MUSE observations are consistent with fine-grained material leaving the system quickest, as expected, as it is pushed away by solar radiation, with larger particles lingering longer (Li et al. 2023; Opitom et al. 2023). We estimate the acceleration due to solar radiation pressure using

$$a_{\rm srp} = \frac{3L_\odot}{16\pi c R_\odot^2 \rho r} Q_{\rm srp}, \quad (1)$$

where the density of the dust grains ρ is assumed to be 3000 kg m^{-3} for S-type asteroid material, the coefficient $Q_{\rm srp} \approx 1$ for grains larger than the dominant wavelengths of sunlight, and we take the solar distance $R_\odot$ as a constant (at its average value of 1.03 au) over the time frame considered here. We find that grains of radius $r = 1$ μm are accelerated to a projected distance of >5″ (more than 340 km along the anti-Sun direction) by the time of the first postimpact observations, assuming that they had zero initial velocity relative to Didymos (so, in an abstract scenario of a dust cloud comoving with the system). This means that these would have already left the photometric apertures used, and therefore the brightening of small grains at increasing phase angle can be ignored in explaining the overall brightness evolution. The picture is complicated by the fact that the ejecta clearly had nonzero initial velocities, and that material ejected into the cone oriented opposite DART's impact velocity, which was approximately Sunward (see Section 4), will first be decelerated before passing through the photometric aperture on its way into the tail direction. This is a proposed explanation for the peak in brightness 8 days after impact (Li et al. 2023), but a significant amount of micron-sized grains would have had to have an initial Sunward velocity of ∼350 m s^{-1} to be accelerated back past the asteroid at +8 days from impact, and would have reached a projected >15′ in the Sunward direction before turning back, filling the DFOSC field of view, which does not match the observed extent of the dust. This is size dependent: 10 μm grains could explain an +8 day bump with initial velocities and maximum Sunward extents 10 times lower, which are a better match to the observed morphology.

In principle, one could calculate the total brightness within an aperture at a given time by summing the contribution over

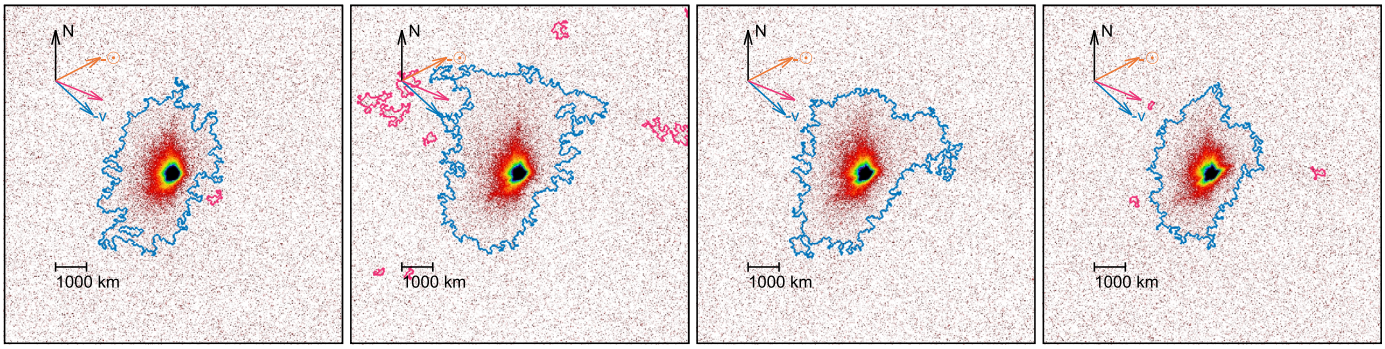

(a) 03:04:32.807 - 03:50:13.575 (b) 03:51:59.420 - 04:49:00.847 (c) 04:49:38.319 - 05:44:20.656 (d) 05:45:12.698 - 06:36:30.803

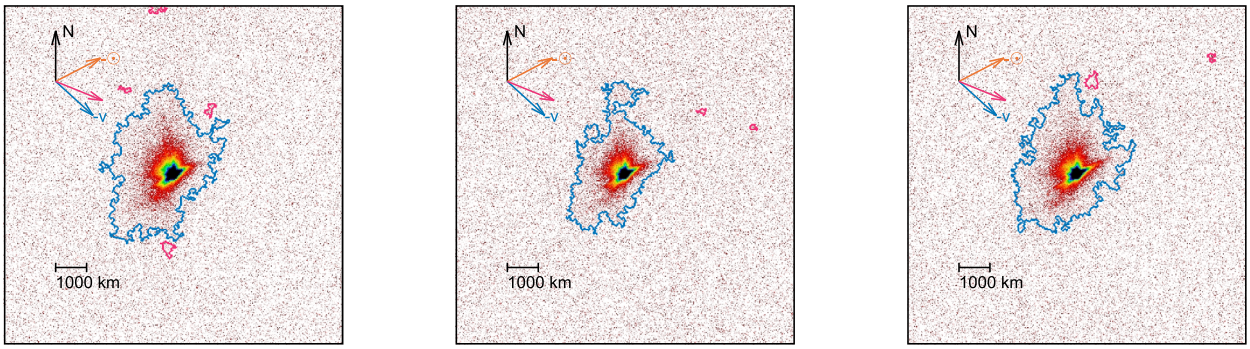

(e) 06:37:27.336 - 07:42:55.663 (f) 07:43:54.735 - 08:41:01.763 (g) 08:41:53.566 - 09:48:05.157

Figure 3. Ejecta evolution in the DK images over the first observing night postimpact. The dominant feature in these images is the ejecta cone, fanning out in the direction from which the DART probe arrived. The tail extending in the antisolar direction can be seen forming in panels (d)–(g). Each panel represents a stack of images with the exposure start UT time on 2022 September 27 for the first and last frame in each sequence included in the panel captions; individual images were exposed for 7 s. Each image stack was produced by aligning images on Didymos, taking a 501 × 501 pixel cutout and then taking the sigma-clipped mean of the corresponding pixels in each image. The color scale goes from white and red for low values to dark blue and black for high values; the minimum and maximum mapped pixel values are taken to be 0.5σ below and 25σ above the mean pixel value in each stack. The *NoiseChisel* detection contours are overlain on the images; the blue outline marks the specific detection that includes the asteroid plus the ejecta, and magenta outlines all other detections. The arrow set in the corner of the image represents north (black arrow labeled "*N*," east is to the left), the antisolar direction (orange, "⊙"), the direction opposite to the system's projected orbital velocity (blue, "*v*"), and the direction from which the DART probe approached the system (unlabeled magenta arrow). Image scale is indicated with a ruler corresponding to 1000 km at the asteroid system.

different grain size bins as

$$f(t) = \sum_r N(r)\zeta(r, t)\pi r^2 p_V \Phi(r, \alpha), \quad (2)$$

where $N(r)$ is the initial population of grains of a given size, $\zeta(r, t)$ describes the fraction remaining in the aperture at time t, p_V is the single scattering albedo of the grains (assumed to be the same for all grains), and $\Phi(r, \alpha)$ is the size-dependent phase integral. For an assumed initial size distribution of ejecta with a continuous power-law form $N(r) \propto r^{-q}$ this relationship should be integrable. In practice there are too many unknowns within ζ (primarily the 3D distribution of initial velocities, and any size dependence on those) for this to be of much use in fitting the fading relationship seen in Figure 2. Modeling the full motion of ejecta is beyond the scope of this work, but has been tackled by others (e.g., Moreno et al. 2023).

4. Morphology

Across the 18 days we observed postimpact the morphology of the ejecta cloud changed in dramatic ways. The detailed structure of the ejecta cloud changed across the 7 hr that we observed it on the first night, as illustrated in the seven panels in Figure 3 (north is up in those images, and east to the left). Over the first night the dominant feature is the ejecta cone fanning out in the direction from which the DART probe arrived (at position angle = 68°, counted from north through east; Cheng et al. 2023). The ejecta cone has a wide opening angle: one edge of the ejecta cone is projected almost exactly north in the images, while the other is southeast, extending almost Sunward. The 18 panels in Figure 4 correspond to all of the images collected on each night deep-stacked to highlight the ejecta features. The Sunward edge of the cone can be seen growing over the first few days postimpact and then gradually dissipating and shrinking as the solar wind pushes the material back. The northern edge of the ejecta cone also dissipates over the course of our observations as the material gets pushed approximately westward. The tail extending in the antisolar direction, as marked by the direction of the orange arrow in Figures 3 and 4, that is clearly visible in later days can be identified by the end of the first postimpact night. There are also fragments of dust cloud moving away from Didymos and slowly dispersing. By the second night postimpact the ejecta tail is very clearly visible and spanning at least 320 pixels (about 7000 km). HST observations from October 8 and 11 clearly show a "double-tail" feature (Li et al. 2023). We cannot resolve this feature in our observations that early, but it can be seen in images taken on October 13 and 14.

We used the *NoiseChisel* procedure (from the *Gnuastro* suite) to establish an approximate outline of the ejecta cloud in the

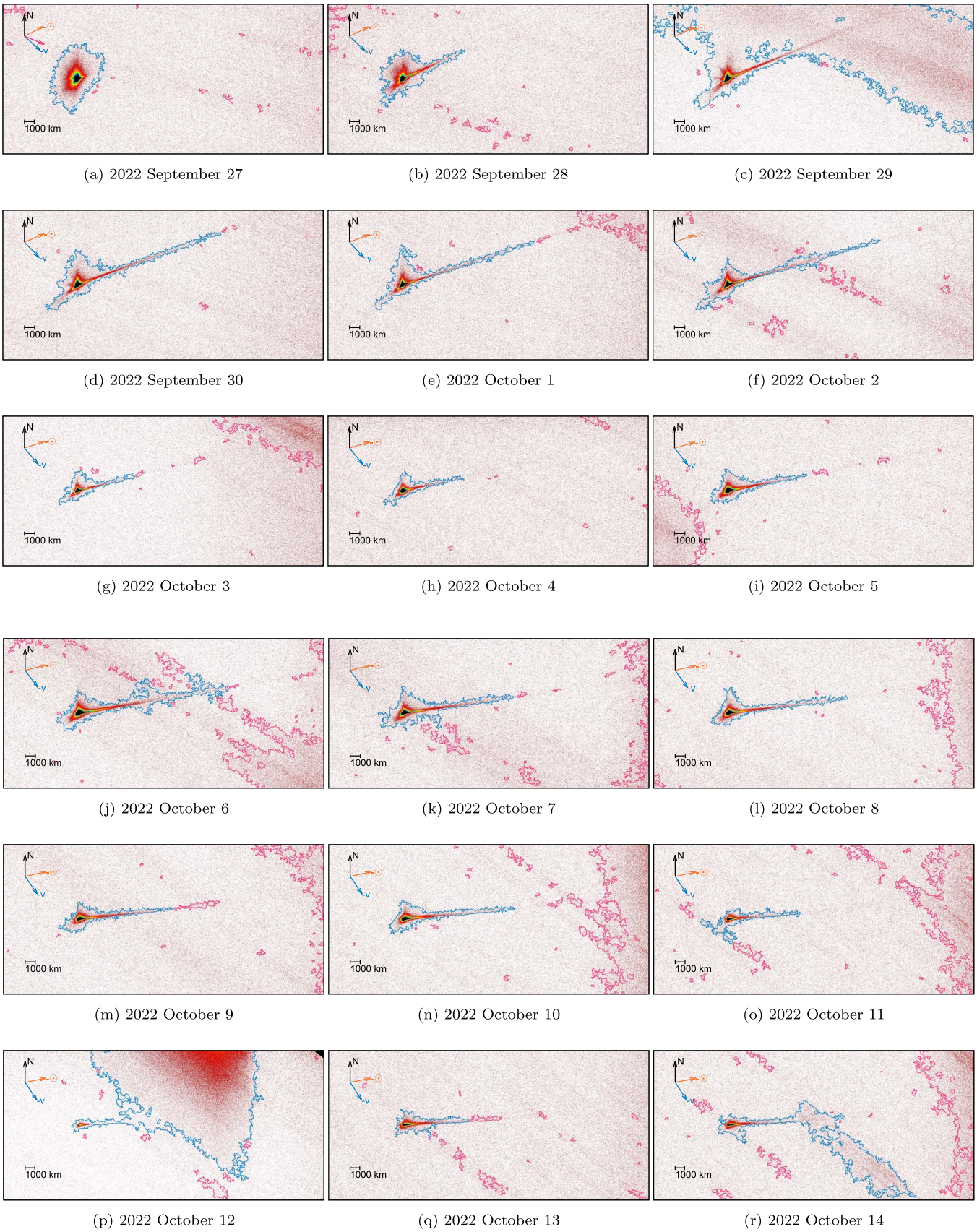

(a) 2022 September 27 (b) 2022 September 28 (c) 2022 September 29

(d) 2022 September 30 (e) 2022 October 1 (f) 2022 October 2

(g) 2022 October 3 (h) 2022 October 4 (i) 2022 October 5

(j) 2022 October 6 (k) 2022 October 7 (l) 2022 October 8

(m) 2022 October 9 (n) 2022 October 10 (o) 2022 October 11

(p) 2022 October 12 (q) 2022 October 13 (r) 2022 October 14

Figure 4. Illustration of the ejecta cloud and tail evolution throughout our postimpact observing campaign. The tail extending in the antisolar direction (indicated with the orange arrow) can seen forming in panels (a) and is clearly identifiable through the rest of our campaign. Each frame is a 1501 × 701 pixel cutout, created by stacking all the images taken throughout each night in the intervals listed in Table 1. The captions for individual panels denote the UT date the observations were taken. The stacking was done through aligning all images taken on a given night and then taking the sigma-clipped mean of the corresponding pixels. More details in caption for Figure 3.

stacked images. The outline of detections containing the Didymos–Dimorphos system are marked with blue lines in Figures 3 and 4. We present approximate measurement of the Sunward ($l_{\odot}$) and antisolar ($l_{-\odot}$) extents of the ejecta cloud in Table 2. These were made using the contours of detections made on the 1501 × 701 image stacks, as shown in Figure 4. While useful for qualitative illustration of the cloud extent and particularly informative when it comes to the changing morphology of the ejecta cloud Sunward extent (for example Figures 4(c), (d), and (e)) even using this method we are not able to separate fully the faint antisolar tail from the background noise; for example in the observations from October 5 (Figure 4(i)) the tail detection is broken into several disjointed detections. The brighter background stars also somewhat interfere with the detections (for example Figures 4(j) and (o)).

The maximum Sunward extent of the ejecta cloud estimated with this method is around 4000 km, and there remain ejecta in this direction throughout the period of observation, suggesting that the ejecta are not dominated by small grains. Micron-sized grains would have cleared over the weeks of observation, or would have extended further toward the Sun if given sufficient initial velocity to still be present at least 8 days after impact, as discussed above. Grains of around 100 μm in size and initial Sunward velocities of 5–10 m s^{-1} would have approximately the right extent and lifetime. However, there must be a faster-moving component (∼100 m s^{-1}) within the ejecta, as the cloud is already more than 3000 km in extent in both the Sunward and anti-Sun projected directions only 7 hr after the impact. The growth of the tail (already more than 6000 km in length by the second night) is consistent with the material at the end of it being of micron sized and accelerating under solar radiation pressure. This material would quickly accelerate to distances greater than those measured over the following nights, but it is worth noting that the antisolar direction "tail" lengths are all minimum values, and the true tail rapidly extends beyond the field of view of DFOSC at a flux level below that which can be separated from the background with statistical significance.

5. Discussion and Conclusions

The brightness decay rate we observe for the ejecta (Section 3) agrees with observations from other observatories (Graykowski et al. 2023; Kareta et al. 2023) and is consistent with material slowly leaving the aperture due to acceleration by solar radiation pressure. While the fast growth of the tail we observe is consistent with it containing particles down to micron size (Section 4), Finson–Probstein modeling by Lin et al. (2023) suggests the dominant ejecta grains to be considerably larger, in the millimeter to centimeter size range. These authors find an expansion velocity in the anti-Sun (tail) direction of 31 m s^{-1} on September 27, consistent with acceleration of millimeter–centimeter particles by radiation pressure, but our deeper images (acquired approximately 14 hr earlier from Chile, versus Lin et al. 2023's observations from Lulin observatory in Taiwan) already show a longer tail. More detailed Monte Carlo modeling of the ejecta motion by Moreno et al. (2023) fits the ejecta using a broken power-law size distribution between micron and 5 cm radius particles. They find a model that contains two components (low and high velocity, ejected hemispherically and into an ejecta cone, respectively), with a third component needed to explain the appearance of the second tail. Both Lin et al. (2023) and Moreno et al. (2023) agree that this secondary dust release event is necessary to produce this tail and that the timing of this is consistent with the "bump" in the photometry we observe around 8 days after impact. Interestingly, an alternative model demonstrating the secondary tail to be an effect of changing viewing geometry of the ejecta cone created in the initial impact event was recently presented by Kim & Jewitt (2023), but it is inconsistent with the ≈8 day brightening we note (Section 3 and Figure 2). The initial velocities in the Monte Carlo model by Moreno et al. (2023) are considerably lower than those we find necessary, of order of 1 m s^{-1} even for the "fast" component. While these provide good fits to the long-term evolution of the ejecta cone and tails seen in their imaging with small telescopes, such low velocities cannot explain the extend of 1000s of kilometers of the ejecta cloud we see in our deep-stacked images on the first nights after impact (Section 4 and Figure 4). In situ observations by LICIACube (Dotto & Zinzi 2023; Dotto et al. 2023) also favor higher ejecta speeds, of order 10s of meters per second for most of the clumps they see, and 300–500 m s^{-1} for faster streamers, which would be consistent with the expansion we see. Finally, it is worth noting that even though the photometric contribution from the ejecta fades to almost nothing over the short span of our observations (and fades completely shortly after, in about 20 days; Lister et al. 2023; Moskovitz et al. 2023), the tail persists. These observations are therefore consistent with asteroid collisions being one of the mechanisms behind observed main-belt asteroid activity. It is direct confirmation that while it would be difficult to observe a quickly dispersing ejecta cloud or brightness enhancement, which are only present for a few days after an impact, a dust tail can be observed long after the event.

To summarize:

1. We report observations of the Didymos–Dimorphos asteroid system collected in 2022 September and October with the DK 1.54 m telescope at La Silla. The photometric measurements contributed to the already reported orbital period change detection (Thomas et al. 2023), but here we focused on the long-term development of the system's brightness and the ejecta morphology.
2. Accounting for changing observing geometry the system exhibits excess brightness compared to earlier photometric models, which comes from the ejecta cloud. The brightness of the ejecta cloud decreases postimpact, increases shortly around 8 days after impact, and then continues to fade at a slower rate than before day eight. Those measurements are consistent with measurements at other observatories and with a secondary impact scenario. The dust tail forms in the first hours after impact and persists for weeks.
3. We used *Gnuastro* and *NoiseChisel* to characterize morphological features of the dust cloud. We are able to assess the minimum extent of the ejecta cloud in both the Sunward and antisolar directions, consistent with small dust grains ejected at 10s to 100s of meters per second, similar to the velocities measured by LICIACube.

Acknowledgments

We thank the two anonymous referees for their kind comments which helped to improve the presentation of our results. We thank all the staff at the ESO La Silla Observatory for their support. A.R. and C.S. acknowledge support from the UK Science and Technology Facilities Council. This project has received funding from the European Union's Horizon 2020 research and innovation program under grant agreement No.

870403 (NEOROCKS). This work was supported by the DART mission, NASA Contract No. 80MSFC20D0004. This research has received funding from the Europlanet 2024 Research Infrastructure (RI) program. The Europlanet 2024 RI provides free access to the world's largest collection of planetary simulation and analysis facilities, data services and tools, a ground-based observational network, and a program of community support activities. Europlanet 2024 RI has received funding from the European Union's Horizon 2020 research and innovation program under grant agreement No. 871149. N.P. acknowledges funding from Fundação para a Ciência e a Tecnologia (FCT), Portugal, through the research grants UIDB/04434/2020 and UIDP/04434/2020. P.L.P. was partly funded by Programa de Iniciación en Investigación-Universidad de Antofagasta. INI-17-03. U.G.J., M.A., and F.A. acknowledge support from the European Union H2020-MSCA-ITN-2019 under grant No. 860470 (CHAMELEON) and the Novo Nordisk Foundation Interdisciplinary Synergy Programme grant No. NNF19OC0057374. D.B.L. and N.S.C. B. who are associated as co-authors of this manuscript are students of the program "Magíster en Astronomía" (Universidad de Antofagasta). This paper uses Paul Tol's color schemes and templates: https://personal.sron.nl/~pault/. For the purpose of open access, the author has applied a Creative Commons Attribution (CC BY) licence to any Author Accepted Manuscript version arising from this submission.

Facility: Danish 1.54 m telescope.

Software: Astropy (Astropy Collaboration et al. 2013, 2018, 2022) and Gnuastro (Akhlaghi & Ichikawa 2015; Akhlaghi 2019).

Appendix
Additional Table and Figures

We include here the full photometric light curves collected for the Didymos–Dimorphos system, collected with the DK 1.54 m between 16 September and 14 October 2022. We include all the photometric measurements callibrated to the ATLAS-RefCAT2 r band in Table A1. We present the preimpact light curves in Figure A1, and the postimpact measurement in Figure A2.

Table A1
Optical Light Curves of the Asteroid (65803) Didymos Collected with the DK 1.54 m Telescope

JD (day)	r (mag)	Δr (mag)	Seg. ⋯	Ap. ($''$)
2459838.848829	14.571	0.004	01	1.5
2459838.849275	14.597	0.005	01	1.5
2459838.849729	14.570	0.003	01	1.5
2459838.850193	14.556	0.004	01	1.5
2459838.850637	14.556	0.004	01	1.5

Notes. The columns are "JD" in days, the time at midexposure with no light-time correction; "r" in mag, callibrated to the ATLAS-RefCat2 r band; "Δr" in mag, the 1σ uncertainty in the magnitude; "Seg.," a numerical label indicating which "Segment" or constant-background star field in a given night the measurement belongs to; and "Ap." in arcseconds, the diameter of the aperture for the measurements. The table is sorted by aperture size first and JD second.

(This table is available in its entirety in machine-readable form.)

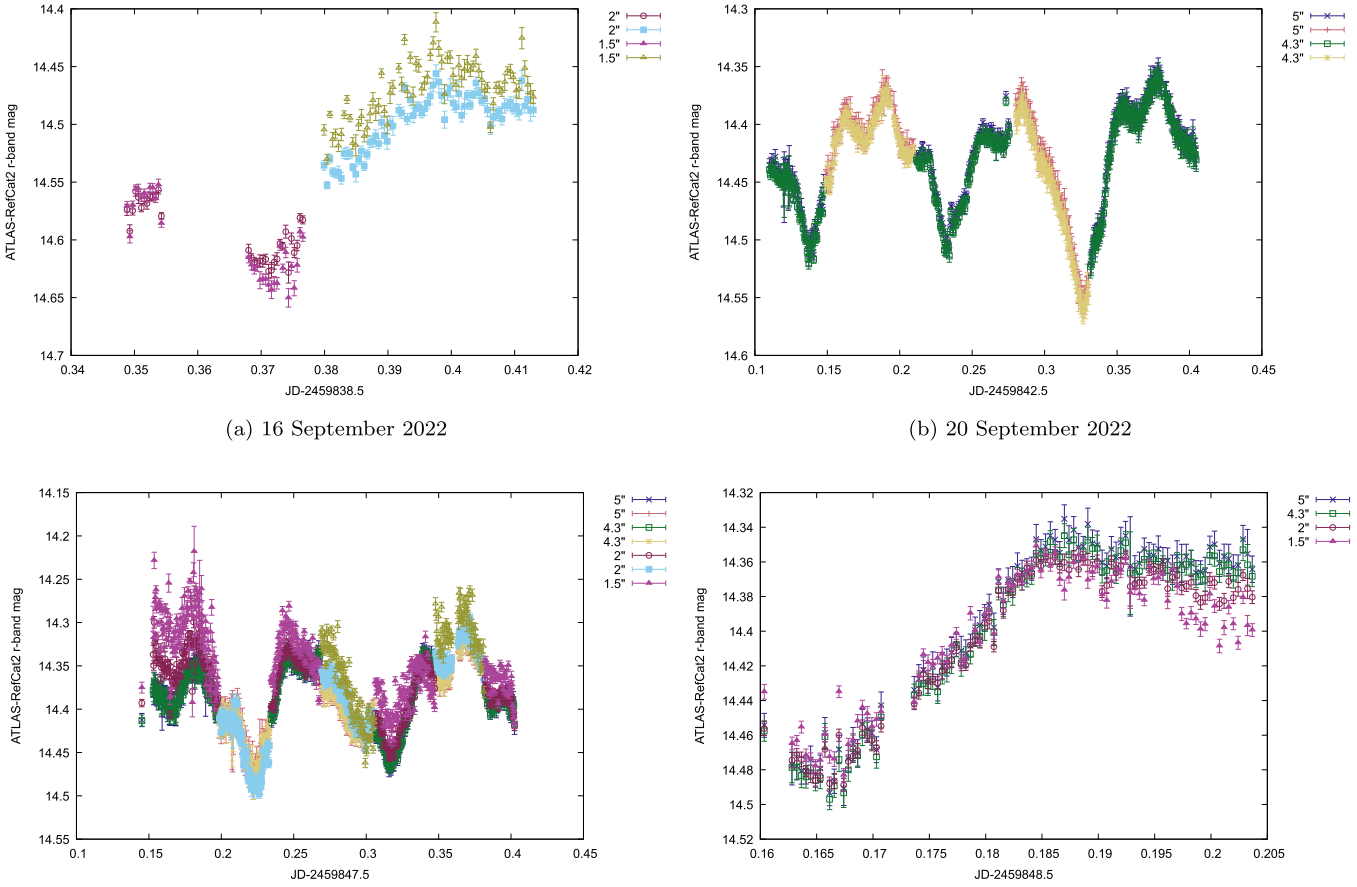

(a) 16 September 2022

(b) 20 September 2022

(c) 25 September 2022

(d) 26 September 2022

Figure A1. Preimpact light curves collected at the DK telescope, calibrated to the ATLAS-RefCat2 *r* band. The horizontal axis scale is in days since 00:00 UT of a given observing night. Each night is divided into "segments" corresponding to different background fields used for relative light-curve extraction. Each segment is marked with a different color and symbol. Due to low seeing and corresponding high noise in small apertures on September 19, plots of the light curves in the 1.″5 and 2″ apertures are omitted on that date.

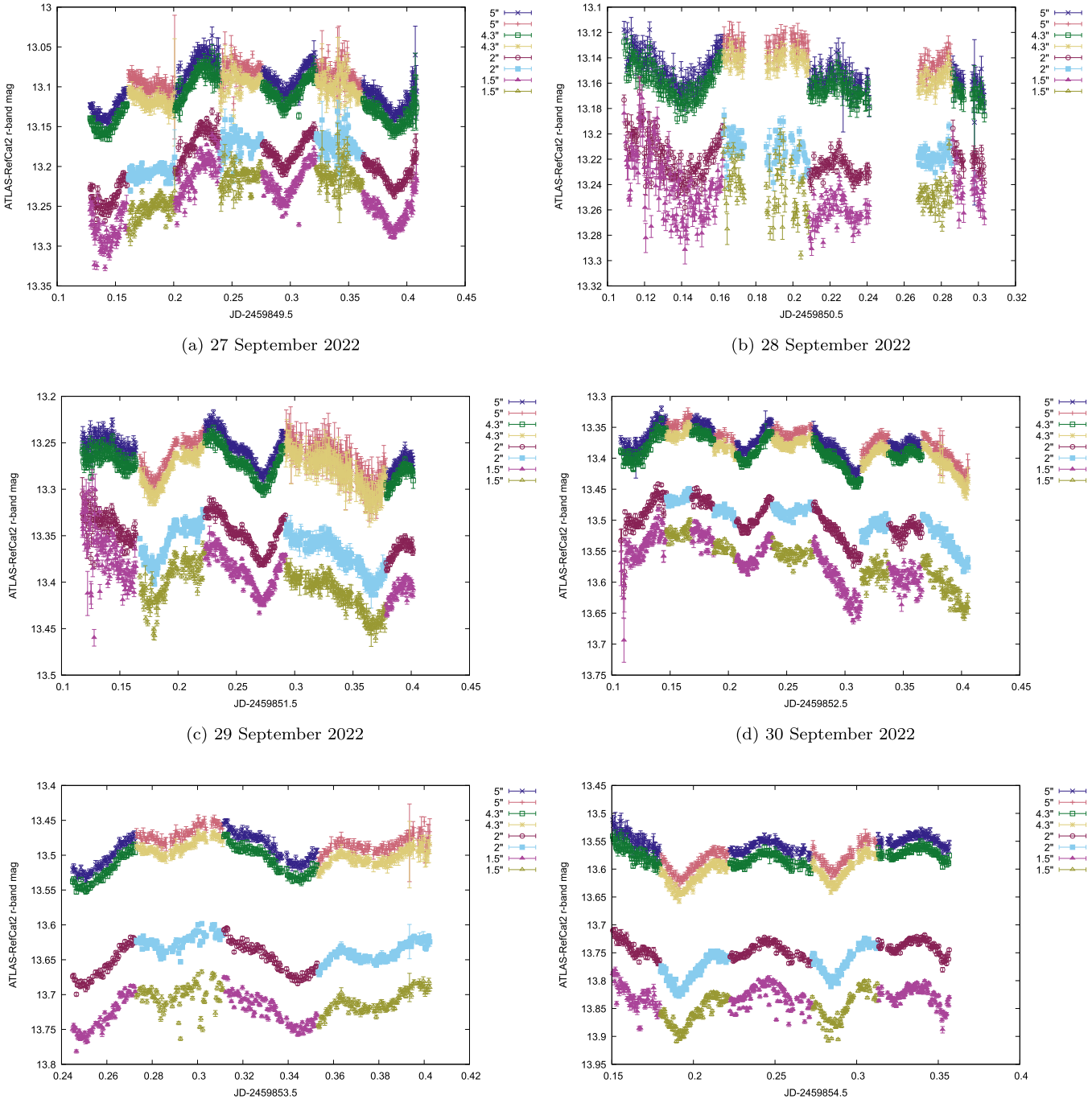

(a) 27 September 2022

(b) 28 September 2022

(c) 29 September 2022

(d) 30 September 2022

(e) 1 October 2022

(f) 2 October 2022

Figure A2. Postimpact multiaperture light curves collected at the DK telescope, calibrated to the ATLAS-RefCat2 *r* band. The horizontal axis scale is in days since 00:00 UT of a given observing night. Each night is divided into "segments" corresponding to different background fields used for the relative light-curve extraction. Each segment and aperture size is marked with a different color and symbol.

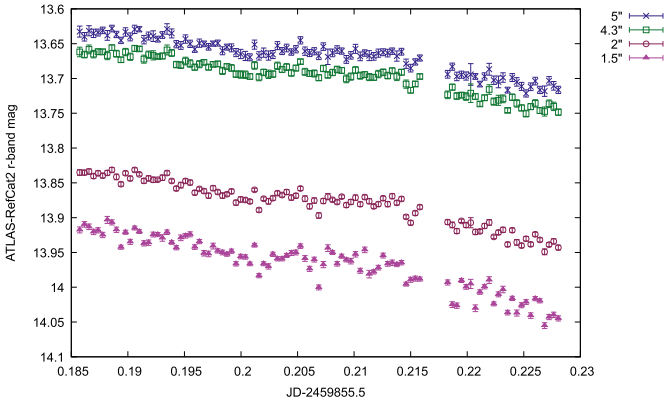

(g) 3 October 2022

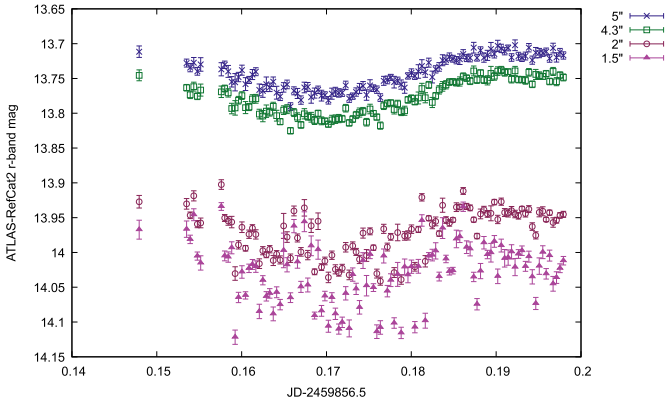

(h) 4 October 2022

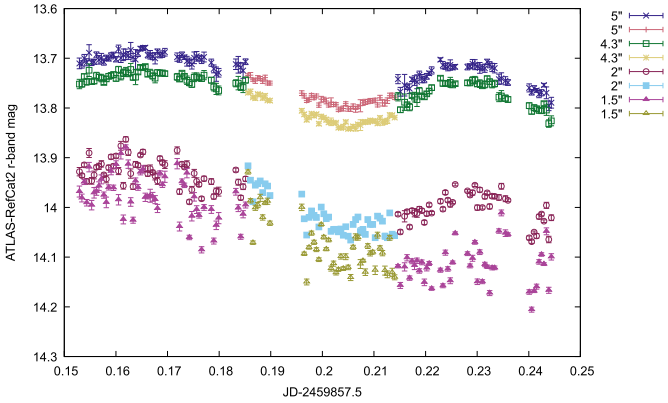

(i) 5 October 2022

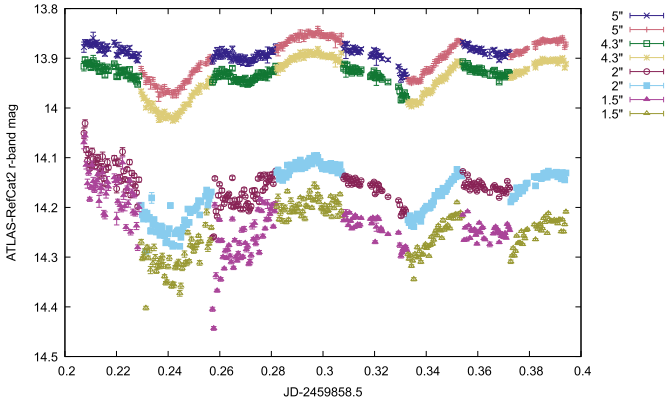

(j) 6 October 2022

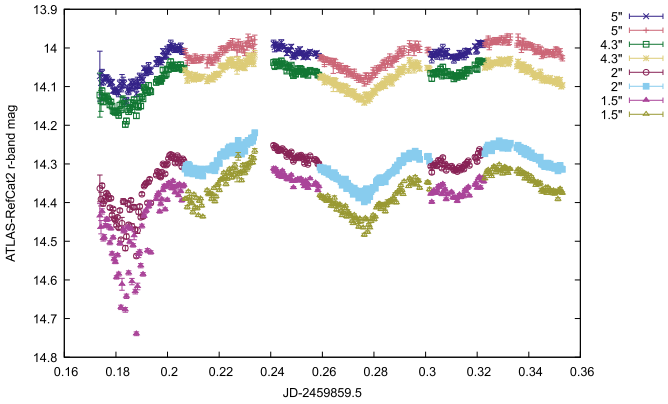

(k) 7 October 2022

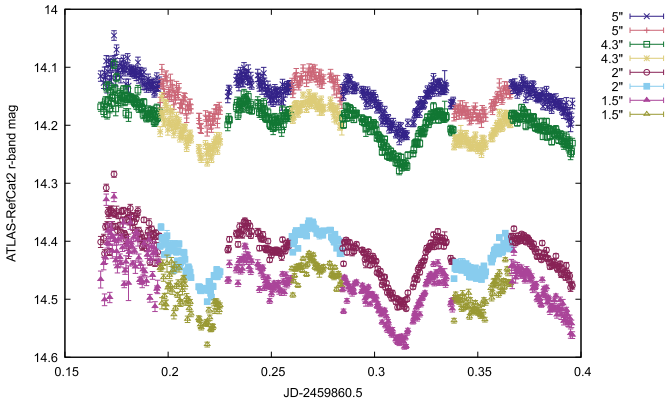

(l) 8 October 2022

Figure A2. (Continued.)

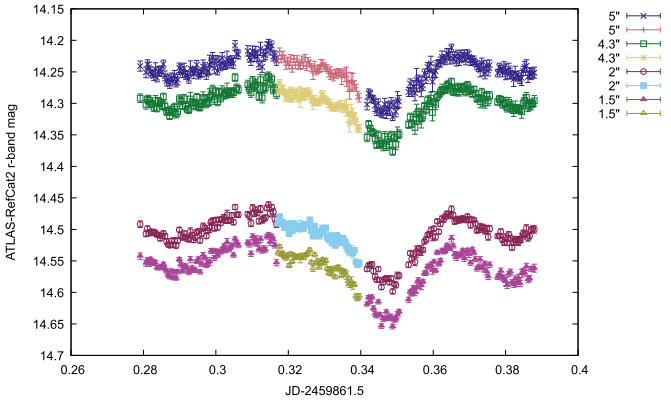

(m) 9 October 2022

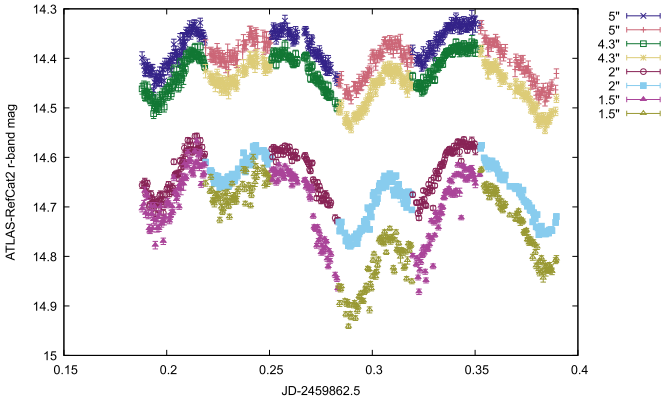

(n) 10 October 2022

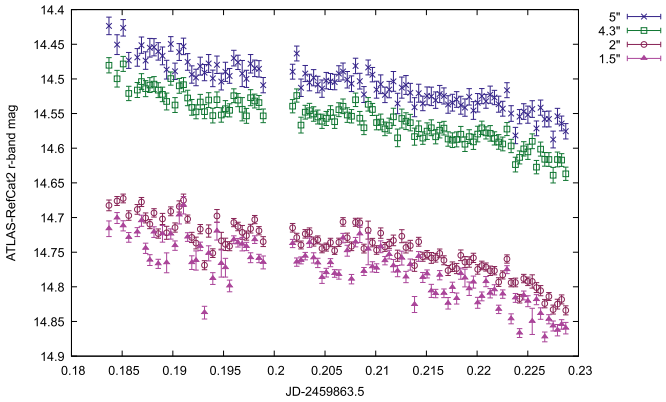

(o) 11 October 2022

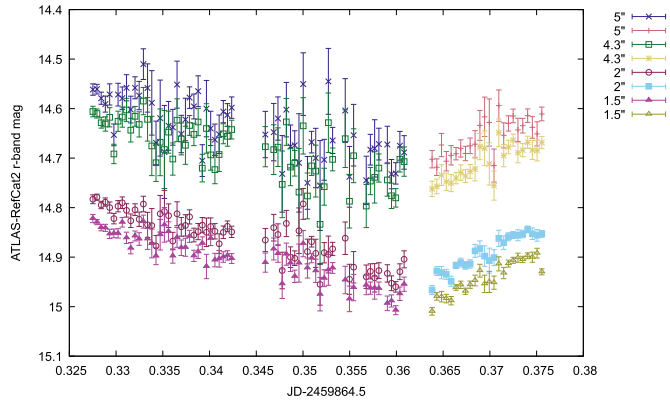

(p) 12 October 2022

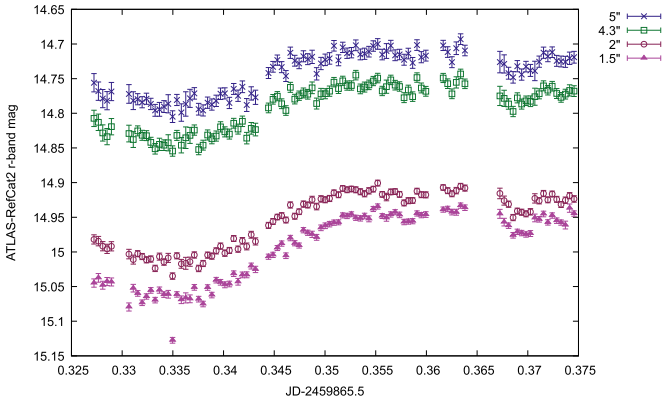

(q) 13 October 2022

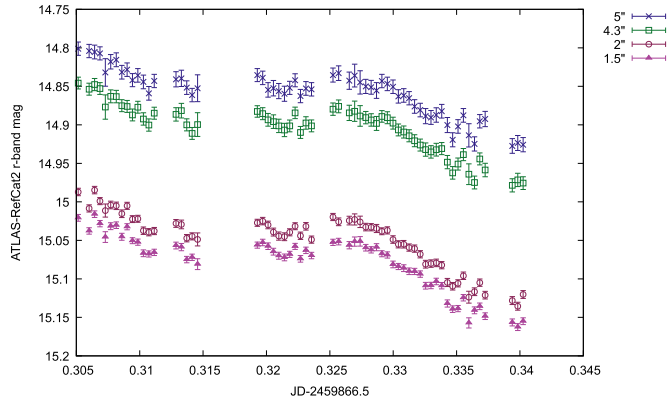

(r) 14 October 2022

Figure A2. (Continued.)

ORCID iDs

Agata Rożek https://orcid.org/0000-0003-2341-2238
Colin Snodgrass https://orcid.org/0000-0001-9328-2905
Uffe G. Jørgensen https://orcid.org/0000-0001-7303-914X
Petr Pravec https://orcid.org/0000-0001-8434-9776
Mariangela Bonavita https://orcid.org/0000-0002-7520-8389
Markus Rabus https://orcid.org/0000-0003-2935-7196
Elahe Khalouei https://orcid.org/0000-0001-5098-4165
Penélope Longa-Peña https://orcid.org/0000-0001-9330-5003
Martin J. Burgdorf https://orcid.org/0000-0002-5854-4217
Abbie Donaldson https://orcid.org/0000-0003-4507-9384
Daniel Gardener https://orcid.org/0000-0002-9925-0426
Sedighe Sajadian https://orcid.org/0000-0002-2859-1071
Valerio Bozza https://orcid.org/0000-0003-4590-0136
Martin Dominik https://orcid.org/0000-0002-3202-0343
J. Fynbo https://orcid.org/0000-0002-8149-8298
Tobias C. Hinse https://orcid.org/0000-0001-8870-3146
Sohrab Rahvar https://orcid.org/0000-0002-7084-5725
John Southworth https://orcid.org/0000-0002-3807-3198
Jeremy Tregloan-Reed https://orcid.org/0000-0002-9024-4185
Mike Kretlow https://orcid.org/0000-0001-8858-3420
Nuno Peixinho https://orcid.org/0000-0002-6830-476X

References

Akhlaghi, M. 2019, arXiv:1909.11230
Akhlaghi, M., & Ichikawa, T. 2015, ApJS, 220, 1
Astropy Collaboration, Price-Whelan, A. M., Lim, P. L., et al. 2022, ApJ, 935, 167
Astropy Collaboration, Price-Whelan, A. M., Sipőcz, B. M., et al. 2018, AJ, 156, 123
Astropy Collaboration, Robitaille, T. P., Tollerud, E. J., et al. 2013, A&A, 558, A33
Cheng, A. F., Agrusa, H. F., Barbee, B. W., et al. 2023, Natur, 616, 457
Daly, R. T., Ernst, C. M., Barnouin, O. S., et al. 2023, Natur, 616, 443
Donaldson, A., Kokotanekova, R., Rożek, A., et al. 2023, MNRAS, 521, 1518
Dotto, E., Deshapriya, J. D. P., Gai, I., et al. 2023, PSJ, submitted
Dotto, E., & Zinzi, A. 2023, NatCo, 14, 3055
Graykowski, A., Lambert, R. A., Marchis, F., et al. 2023, Natur, 616, 461
Jewitt, D., Hsieh, H., & Agarwal, J. 2015, in Asteroids IV, ed. P. Michel, F. E. DeMeo, & W. F. Bottke (Tucson, AZ: Univ. Arizona Press), 221
Jewitt, D., Kim, Y., Li, J., & Mutchler, M. 2023, ApJL, 952, L12
Kareta, T., Thomas, C., Li, J.-Y., et al. 2023, ApJL, in press (arXiv:2310.12089)
Kelley, M. S. P., & Lister, T., 2022 Calviacat: Calibrate star photometry by catalog comparison, Astrophysics Source Code Library, ascl:2207.015
Kim, Y., & Jewitt, D. 2023, ApJL, 956, L26
Kitazato, K., Abe, M., Mito, H., et al. 2004, LPSC, 35, 1623
Li, J.-Y., Hirabayashi, M., Farnham, T. L., et al. 2023, Natur, 616, 452
Lin, Z.-Y., Vincent, J.-B., & Ip, W.-H. 2023, A&A, 676, A116
Lister, T., Constantinescu, C., Ryan, W., et al. 2023, PSJ, submitted
Lolachi, R., Glenar, D. A., Stubbs, T. J., & Kolokolova, L. 2023, PSJ, 4, 24
Michel, P., Ballouz, R.-L., Barnouin, O. S., et al. 2020, NatCo, 11, 2655
Michel, P., DeMeo, F. E., & Bottke, W. F. 2015, in Asteroids IV, ed. P. Michel, F. E. DeMeo, & W. F. Bottke (Tucson, AZ: Univ. Arizona Press), 3
Moreno, F., Campo Bagatin, A., Tancredi, G., et al. 2023, PSJ, 4, 138
Moskovitz, N., Thomas, C., Pravec, P., et al. 2023, PSJ, in press (arXiv:2311.01971)
Murphy, B., Opitom, C., Snodgrass, C., et al. 2023, PSJ, in press (arXiv:2311.09977)
Nesvorný, D., Brož, M., & Carruba, V. 2015, in Asteroids IV, ed. P. Michel, F. E. DeMeo, & W. F. Bottke (Tucson, AZ: Univ. Arizona Press), 297
Opitom, C., Murphy, B., Snodgrass, C., et al. 2023, A&A, 671, L11
Polishook, D., DeMeo, F. E., Burt, B. J., et al. 2023, PSJ, 4, 229
Pravec, P., Harris, A. W., Kušnirák, P., Galád, A., & Hornoch, K. 2012, Icar, 221, 365
Pravec, P., Scheirich, P., Kušnirák, P., et al. 2006, Icar, 181, 63
Pravec, P., Thomas, C. A., Rivkin, A. S., et al. 2022, PSJ, 3, 175
Rivkin, A. S., Chabot, N. L., Stickle, A. M., et al. 2021, PSJ, 2, 173
Scheirich, P., Pravec, P., Meyer, A., et al. 2023, PSJ, submitted
Schleicher, D. G., & Bair, A. N. 2011, AJ, 141, 177
Thomas, C. A., Naidu, S. P., Scheirich, P., et al. 2023, Natur, 616, 448
Tonry, J. L., Denneau, L., Flewelling, H., et al. 2018, ApJ, 867, 105
Tonry, J. L., Stubbs, C. W., Lykke, K. R., et al. 2012, ApJ, 750, 99
Walsh, K. J. 2018, ARA&A, 56, 593